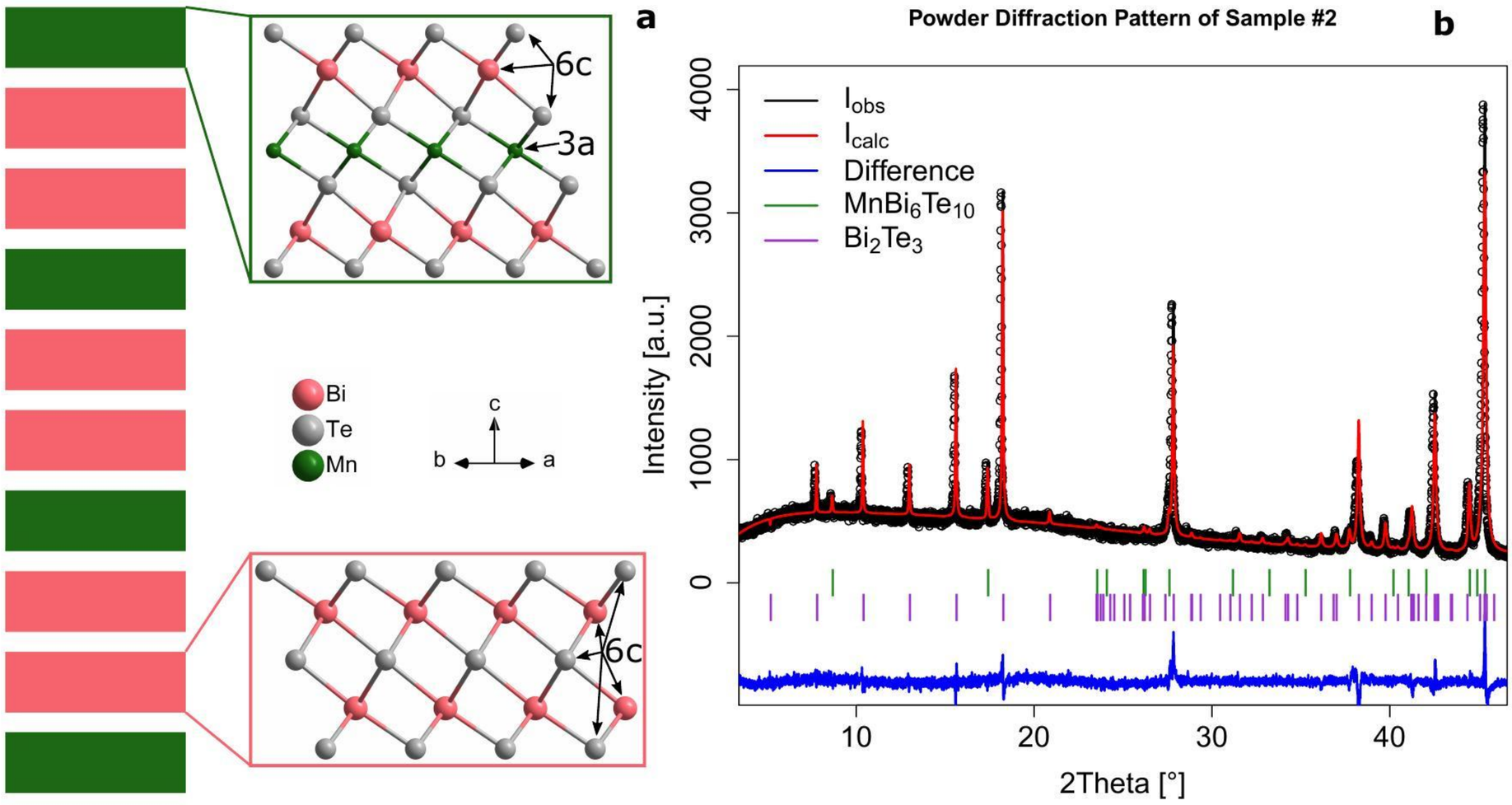

FIG. 1. Crystal structure properties. a) The unit cell of $MnBi_6Te_{10}$ is sketched by slabs of red and green boxes, where green indicates a septuple layer and red indicates a quintuple layer. In the expanded views we show the atomic structure. The QL and SL are interleaved by van der Waals gaps. b) Experimental (black) and refined by Rietveld method (red) powder X-ray diffraction pattern of the sample #2 in the 2θ range $5-45°$. For the full 2θ range, see Fig. S1. The difference curve is shown in blue ($R_p = 0.055$, $wR_p = 0.071$, GoF = 1.48). A small fraction of Bi_2Te_3 comprises 7 wt. % ($R\bar{3}m$, $a = 4.3797(4)$ Å, $c = 30.4965(7)$ Å, $R_{obs} = 0.094, wR_{obs} = 0.096, R_{all} = 0.109$). The main phase is refined with the overall $Mn_{0.8}Bi_{6.2}Te_{10}$ composition ($R\bar{3}m$, $a = 4.3667(2)$ Å, $c = 101.869(4)$ Å, $R_{obs} = 0.079, wR_{obs} = 0.074, R_{all} = 0.104$).

or $Mn_{0.8}Bi_{6.2}Te_{10}$) were introduced as constraints (see Supporting Information sec. I). When cation Mn/Bi intermixing was allowed in the refinement, the reliability factors R_{all} and R_{obs} dropped down significantly, confirming that this phenomenon was undoubtedly present in the structure. Due to very low sample mass (1–2 mg), the acquired powder diffraction data did not allow us to settle in for just one particular intermixing model with a statistically unequivocal quantification. The refined Mn content is also strongly dependent on whether cation vacancies are allowed in the refinement. We opted for a structural solution without voids in the $3a$ and $6c$ positions. Despite the outlined uncertainties, all tested models with various composition constraints have in common that: 1) the Mn:Bi ratio in the $3a$ position in the center of an SL is close to 56:44; 2) the outer cation site of an SL ($6c$) contains up to 2 % Mn; 3) the QL always accommodates some Mn (2–7 % Mn) in the $6c$ cation sites. The presence of Mn in all cation positions accords with our earlier reported refinement on $Mn_{0.81}Bi_{6.13}Te_{10}$ single crystals [31] and is in contrast to the findings of Klimovskikh *et al.* [23]. Such subtle variations in intermixing patterns can dramatically impact the magnetic properties, as witnessed in the next subsection.

B. Bulk magnetometry

Fig. 2a shows the field-cooled (FC) and zero-field cooled (ZFC) normalized magnetization of sample #2 in an out-of-plane magnetic field of 10 mT. A phase transition into a long-range magnetically ordered state is observed at $T_c = 12.0$ K, determined by the inflection point, together with a notable FC/ZFC splitting around 10 K. These observations point towards a ferromagnetic alignment of the Mn spins in our $MnBi_6Te_{10}$ samples and contrast with the antiferromagnetic transition at $T_N \sim 11$ K so far reported for the nominal $MnBi_6Te_{10}$ composition [23, 25, 27, 33, 34]. Our Curie-Weiss analysis in the temperature regime 100–400 K (see inset of Fig. 2a and Sec. IV) yields an effective moment of $m_{\text{eff}} = 5.8 \pm 0.1\ \mu_B$/Mn in close agreement with the value $m_{\text{eff}} = 5.67\mu_B$ calculated by multiplet ligand-field theory (MLFT) (sec. II E). The uniformity of all four $MnBi_6Te_{10}$ crystals is strongly supported by the nearly identical SQUID magnetometry curves (see Fig. S4), with transition temperatures that vary by only 0.1 K.

The magnetization curves $M(H)$ in Fig. 2b show clear FM loop openings, with a coercive field of $\mu_0 H_c \sim 32$ mT at $T = 2$ K, and a finite remanent moment of $m_{\text{SQ}}^{\text{tot}} = (3.9 \pm 0.2)\mu_B$/Mn at zero magnetic field. The moment at 0.15 T is $m_{\text{SQ}}^{\text{tot}} = (4.2 \pm 0.2)\mu_B$/Mn.

It is furthermore interesting to compare our results to analogously synthesized samples of the MBT_n family (Fig. 2c). We observe a noteworthy trend as the num-